Synthesis in Molten Salts and Characterization of Li 6 B 18 (Li 2 O) x Nanoparticles

Simon Delacroix, Yann Le Godec, Cristina Coelho, Christel Gervais, Isabelle Genois, Patrick Legriel, David Portehault

Synthesis in molten salts and characterization of $Li_6B_{18}(Li_2O)_x$ nanoparticles

Simon Delacroix,[1,2] Yann Le Godec,[2,*] Cristina Coelho-Diogo,[3] Christel Gervais,[1] Isabelle Génois,[1] Patrick Le Griel,[1] David Portehault[1,*]

[1] *Sorbonne Université, CNRS, Collège de France, Laboratoire de Chimie de la Matière Condensée de Paris (CMCP), 4 place Jussieu, F-75005, Paris, France*

[2] *Sorbonne Université, CNRS, MNHN, IRD, Institut de Minéralogie, de Physique des Matériaux et de Cosmochimie (IMPMC), 4 place Jussieu, F-75005, Paris, France*

[3] *Sorbonne Université, CNRS, Institut des Matériaux de Paris Centre (IMPC), 4 place Jussieu, F-75005, Paris, France*

*Corresponding authors:

david.portehault@sorbonne-universite.fr

yann.le_godec@sorbonne-universite.fr

Abstract

Lithium borides have been synthesized exclusively through classical solid-state chemistry processes that lead to bulk materials. Indeed, due to the lack of reactivity of the solid boron precursors usually employed and to the high covalent connectivity in such solids, high temperatures and long reaction times are necessary to obtain lithium borides. These conditions result in extensive crystal growth. Here we present the synthesis of nanoparticles of a lithium boride bearing tunnel-like cavities templated by neutral Li_2O species, which have been reported to be labile. To reach this goal, a liquid-phase synthesis in inorganic molten salts has been developed. The $Li_6B_{18}(Li_2O)_x$ nanoparticles have been characterized by scanning and transmission electronic microscopy (SEM and TEM), X-ray diffraction (XRD), and Raman spectroscopy. We provide an in-depth structural characterization by using ^{1}H, ^{7}Li, and ^{11}B solid-state nuclear magnetic resonance (NMR) coupled with DFT modeling to provide the first assignment of ^{7}Li and ^{11}B solid-state NMR signals in lithium borides. We then assess the nanoparticle morphology oriented along the direction of the cavities. This feature shows similarities with structurally related hexagonal tungsten bronzes and could therefore affect the electrochemical and ion exchange properties.

Introduction

Only four of the many crystalline lithium borides discussed in the literature have been fully structurally described[1]. Indeed, the determination of the exact structure and composition of these compounds is made difficult by the fact that they are formed of only light elements. Three lithium borides were synthesized and fully characterized by Nesper and his collaborators: Li_3B_{14},[2] Li_2B_6[3] and LiB_x[4] in 1988, 1999 and 2000, respectively (**Figure 1**). The LiB_x structure proposed by Nesper *et al.* ended the debate on the existence of Li_5B_4[5] and Li_7B_6[6] whose structures were uncorrectedly described. These two solids were in fact particular compositions of the solid solution LiB_x ($x = 0.80$ and $x = 0.85$). The LiB_x structure was solved the same year by Li *et al.*[7] who focused on the particular case of LiB ($x = 1$). On the boron-rich side of the Li-B phase diagram, a lithium boride bearing a lithium intercalated rhombohedral β-boron structure was first described as LiB_{13} in 1988,[8] until its structure was refined as $Li_{30}B_{309}$ in 2009 (**Figure S1** and **S2** in supplementary information).[9] Wörle, Nesper *et al.* discovered another compound in 2007: $Li_6B_{18}(Li_2O)_x$[10] ($0 \leq x \leq 1$). Although this hexagonal phase (space group P6/mmm) contains oxygen atoms, it can be considered as a neutral lithium boride network built on boron octahedra and Li atoms in (Li1 crystallographic position, see details in **Table S1**) and bearing tunnel-like cavities along the *c* axis templated by neutral lithium oxide Li_2O species (**Figure 2A**). This structure is very close to hexagonal tungsten bronzes A_xWO_3 (A=H, Li, Na, K) with B_6 octahedra, B_6-B_6 bonds and Li_2O substituting WO_6, W-O-W bridges and the alkaline cation A^+, respectively.[11,12] In addition to this structure, Li_2O template species are located in the 6-fold channels (**Figure 2**, Li crystallographic positions Li2 and Li3 in yellow and green, respectively). Due to the presence of channels able to exchange ionic and molecular species, these phases are known as molecular sieves. Especially, Wörle, Nesper *et al.* have reported the possibility to remove Li_2O species by washing with water, thus providing empty channels.[13]

All procedures reported to synthesize lithium borides employ bulk boron as precursor (**Table 1**).[2–4,9,10] Due to the lack of reactivity of elemental boron, syntheses require prolonged heating, usually for durations longer than 10 hours. The lithium source is metallic lithium, the volatility of which requires operation in sealed vessels. Lithium is also pyrophoric and requires purification in harsh conditions, by distillation under vacuum.

Herein we describe an alternative route towards $Li_6B_{18}(Li_2O)_x$ based on a liquid-phase synthesis in easy-to-handle molten salts. The use of a liquid medium increases the reaction rate by increasing the frequency of collisions between the reactants and enables working at lower temperature and shorter time compared to most previously reported procedures (**Table 1**). Another consequence is that the nucleation rate of the crystals increases, thus enabling a decrease in the particle size.[14] Herein we report extended characterization of the material, especially by using powder X-ray diffraction, electron microscopy, Raman and ^{1}H, ^{7}Li and ^{11}B solid-state nuclear magnetic resonance. We demonstrate the possibility to synthesize nanoparticles of $Li_6B_{18}(Li_2O)_x$ with well-defined crystal facets and preferential growth along the direction of the tunnel-like cavities.

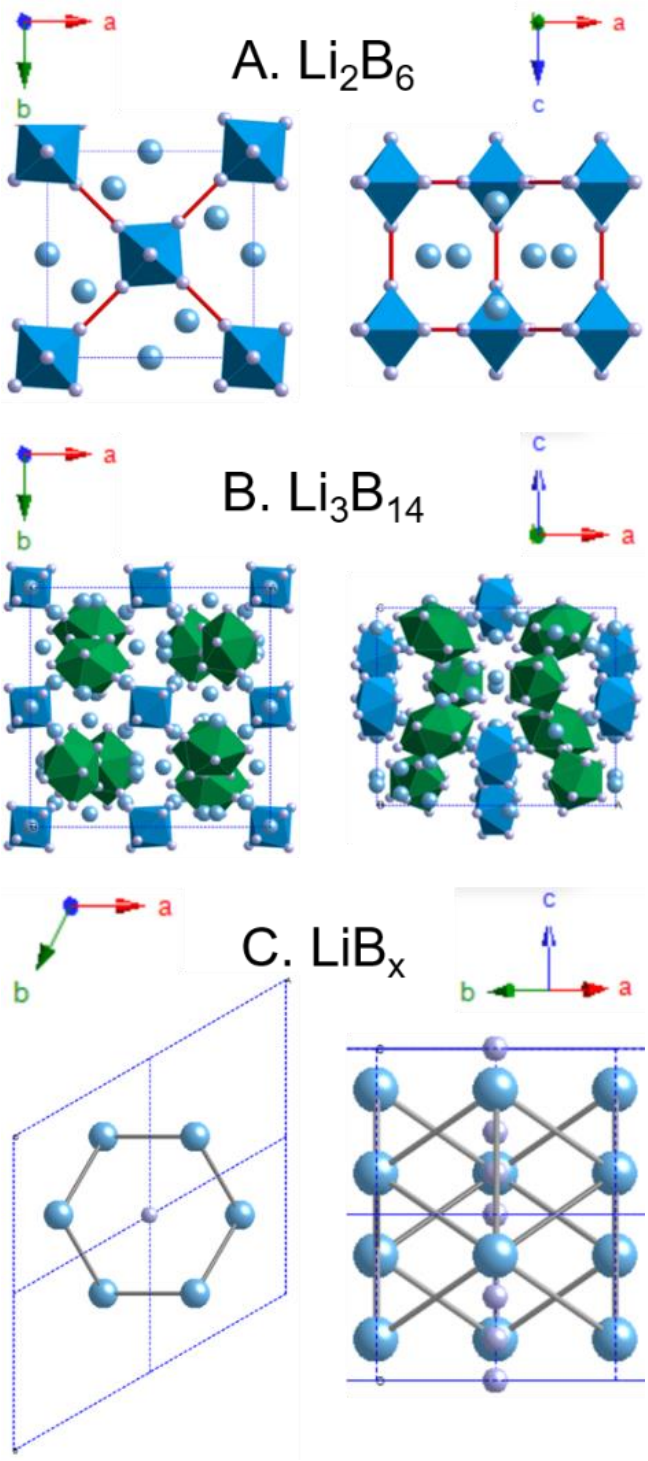

Figure 1. Crystallographic structures of some lithium borides: (A) Li_2B_6, with B_6 octahedra (blue) surrounded by Li atoms (light blue), the interoctahedral bonds are in red. (B) Li_3B_{14} with B_8 (blue) and B_{10} polyhedra (green, bonds between clusters are not shown for the sake of clarity) surrounded by Li atoms (light blue); (C) LiB_x with an infinite chain of boron atoms surrounded by Li atoms (Li and B atoms are in light blue and grey, respectively).

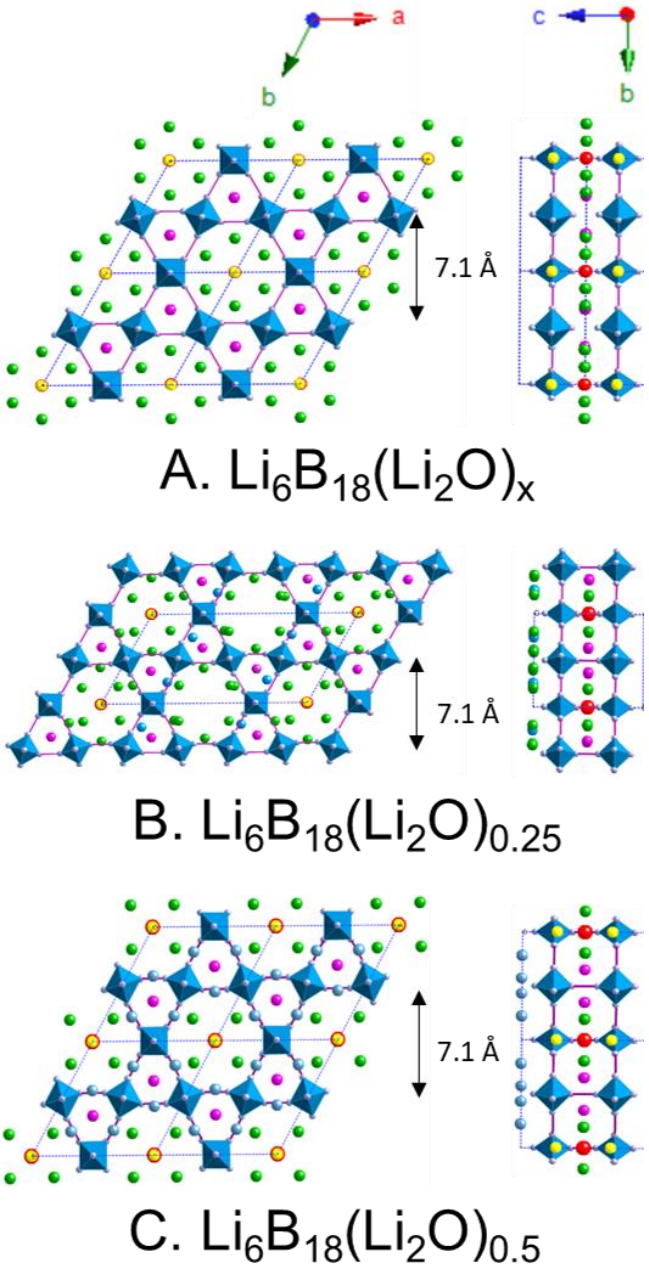

Figure 2. Crystallographic structures of $Li_6B_{18}(Li_2O)_x$ (A) proposed by *Nesper et al.*[10] (B) Structure obtained by DFT relaxation starting from the structure A with x = 0.25 and (C) with x = 0.5. B_6 octahedra are in blue. Boron and oxygen are in grey and red, respectively. Li atoms are in purple, green and yellow, for crystallographic positions Li1, Li2 and Li3 respectively.

Table 1. Synthesis conditions of the different lithium borides reported in the literature.

	Temperature (°C)	Time (h)	Precursors	Method
LiB_x[4]	500	48	Li, β-B	Sealed vessel
Li_2B_6[3]	1500	4	Li, β-B	Sealed vessel
Li_3B_{14}[2]	1427	12	Li, β-B	Sealed vessel
$Li_{30}B_{309}$[9]	1000	12 or 140	Li, β-B	Sealed vessel
$Li_6B_{18}(Li_2O)_x$[10]	900	2	Li_2O, B, Li	Li flux in sealed vessel
$Li_6B_{18}(Li_2O)_x$ (this work)	800	1	$NaBH_4$, LiI (Li_2O)	LiI/KI eutectic mixture in open vessel

Methods

5 g of an eutectic mixture of lithium iodide (99 %, Sigma Aldrich) and potassium iodide (99 %, Alfa Aesar) (58/42 weight ratio) were grinded with 0.6 g of $NaBH_4$ (98 %, Alfa Aesar) during two minutes at 20 Hz (Retsch MM400, 50 mL stainless steel bowls filled with one ball) to obtain a finely ground initial mixture. This mixture was heated to 800 °C at a rate of 10 °C min^{-1} over 1 h in a molybdenum crucible (InnovMetor) inserted in a quartz tube filled by a flow of an inert atmosphere of argon (Ar 99.999%, H_2O <3 ppm, used as received). After the sample was cooled, a black monolith of salts embedding the particles was obtained. The particles were then washed four times with methanol (Normapur grade VWR) by centrifugation − redispersion cycles in order to obtain a black powder. This powder was dried under vacuum at 40 °C during two hours, recovered and stored under argon in a glovebox (H_2O < 0.5 ppm, O_2 < 0.5 ppm). The synthesis was reproduced 10 times to ensure reproducibility. In a typical synthesis, around 160 mg of $Li_6B_{18}(Li_2O)_x$ is isolated, the yield in boron atoms is around 80 %. A byproduct of the reaction is metallic sodium that evaporates in the conditions of synthesis and is deposited on the cold parts of the quartz tube. Although no appreciable reaction was detected when this

deposit was exposed to air, special care should be taken for treatment of this deposit in case of scale-up of the synthesis and then larger amounts of deposited sodium.

Powder XRD was performed on a Bruker D8 Advance diffractometer in the Bragg-Brentano mode at the Cu Kα wavelength. The reference crystallographic structure of $Li_6B_{18}(Li_2O)_x$ was taken from the ICSD database ref Karlsruhe (415266 card). Solid-state MAS NMR spectra were acquired on a Bruker AVANCE III 700 spectrometer with a 16.4T superconducting solenoid operating at ν_0 = 224.68 and 272.16 MHz using commercial triple resonance Bruker MAS probe. Powder samples were transferred to ZrO_2 rotors and spun at a MAS rate of 20 kHz. ^{1}H, ^{7}Li and ^{11}B chemical shifts were referenced to TMS, LiCl and $BF_3.OEt_2$, respectively.

The $Li_6B_{18}(Li_2O)_{0.5/0.25}$ models were obtained starting from the original model proposed by Nesper et al.[10] and using double and quadruple unit cells. Some Li_2, Li_3, and O atoms were removed to be consistent with the expected composition of the system, and all atomic positions were then relaxed with the VASP (Vienna *ab initio* simulation package) code[15] based on the Kohn − Sham density functional theory (DFT) and using a plane-wave pseudopotential approach. The cell parameters were fixed to the X-ray diffraction parameters during geometry optimizations. The NMR parameters were then calculated within the Kohn − Sham DFT using the QUANTUM-ESPRESSO code,[16] keeping the atomic positions equal to the values previously calculated with VASP. The PBE generalized gradient approximation[17] was used, and the valence electrons were described by norm-conserving pseudopotentials[18] in the Kleinman − Bylander form.[19] The shielding tensor was computed using the gauge including projector augmented wave (GIPAW) approach,[20] which enables the reproduction of the results of a fully converged all-electron calculation. The isotropic chemical shift δ_{iso} is defined as $\delta iso = -[\sigma - \sigma_{ref}]$, where σ is the isotropic shielding and σ_{ref} is the isotropic shielding of the same

nucleus in a reference system. In the present case, the comparison is between the experimental δ_{iso} value and calculated δ_{iso} value. ^{11}B and ^{7}Li chemical shift values for B_2O_3 (ICSD entry 16021, δ_{iso} 14.6 ppm) and LiCl (ICSD entry 26909, δ_{iso} 0 ppm) were used. The principal components V_{xx}, V_{yy}, and V_{zz} of the electric field gradient (EFG) tensor defined as $|V_{zz}| \geq |V_{xx}| \geq |V_{yy}|$ were obtained by diagonalization of the calculated tensor. The quadrupolar interaction could then be characterized by the quadrupolar coupling constant C_Q and the asymmetry parameter η_Q, which are defined as $C_Q = eQV_{zz}/h$ and $\eta_Q = (V_{yy} - V_{xx})/ V_{zz}$ (e is the proton charge, h Planck's constant, and Q the quadrupole moment of the considered nucleus). The Q values reported by Pyykkö[21] were used in the calculations for ^{11}B (40.59 mb) and ^{7}Li (-40.03 mb). Calculated spectra were obtained using the DMFit program.[22] Since the calculated quadrupolar coupling constants are very small for both ^{7}Li and ^{11}B sites, Gaussian shapes were used for all components.

SEM and TEM images were recorded on a Hitachi SU-70 microscope and a Technai Spirit 2 microscope, respectively. Raman spectroscopy was performed on the powder with a Kaiser Optical System Raman Analyzer RX1 Microprobe with a 785 nm laser diode.

Results and discussion

The synthesis of $Li_6B_{18}(Li_2O)_x$ was performed by decomposing sodium borohydride in the eutectic mixture LiI/KI (58/42 mass ratio, T_{melt} = 277°C) at 800 °C under argon as described in the methods paragraph. The XRD pattern (**Figure 3**) of the resulting powder shows that $Li_6B_{18}(Li_2O)_x$ is obtained as a pure crystalline phase.

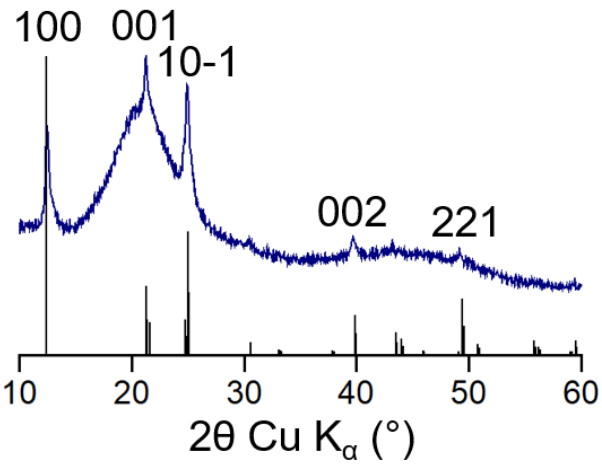

Figure 3. XRD pattern of the powder recovered after molten salts synthesis at 800 °C. The reference pattern of $Li_6B_{18}(Li_2O)_x$ is given in black with the corresponding indexation. The broad peak between 15 and 30 ° is due to beam scattering by the protective PMMA plastic dome used to maintain the powder under protective argon atmosphere.

The $Li_6B_{18}(Li_2O)_x$ structure is confirmed by Raman spectroscopy showing three vibration bands at 735, 1130 and 1250 cm^{-1} (**Figure 4A**). These bands are characteristic of the B_6 clusters with the T_{2G}, E_G and A_{1G} vibration modes, respectively.[23]

^1H, ^7Li and ^{11}B solid-state nuclear magnetic resonance (NMR) spectra were recorded to characterize the local structure. On the ^1H solid-state NMR spectrum (**Figure 4C**), a narrow peak is observed at 0 ppm with an intensity of the same order of magnitude as the rotor signal (circles). This very low intensity peak is attributed to the protons of residual methanol adsorbed at the surface of the particles after the washing and drying steps. No other signal could be detected. Hence, ^1H solid-state NMR confirms that ABH_4 (A=Li, Na, K) hydrides are totally decomposed and methanol is almost totally eliminated from the surface of the particles.

The ^7Li solid-state NMR spectrum shows two different contributions: a main one around 0 ppm and a less intense one around -4 ppm (**Figure 4D**). We could not obtain from the literature any reliable assignment of solid-state NMR signals for lithium borides. Because NMR

is especially suited for the structural study of compounds encompassing light elements as lithium and boron, we have embarked in the calculation of the ^{7}Li and ^{11}B solid-state NMR spectra of $Li_6B_{18}(Li_2O)_x$ with varying *x*. To propose a tentative assignment of the ^{7}Li spectrum, the ^{7}Li NMR parameters were calculated in the two model structures $Li_6B_{18}(Li_2O)_{0.25}$ and $Li_6B_{18}(Li_2O)_{0.5}$ (**Figure 2B** and **2C**). These two structures were obtained starting from the original one proposed by Nesper *et al*[10] showing 3 Li sites with occupancies of 1, 0.665 and 0.644 for Li1, Li2 and Li3, respectively, and one oxygen site with an occupancy of 0.264 (for a global $Li_6B_{18}(Li_2O)_{0.26}$ composition). The $Li_6B_{18}(Li_2O)_{0.25}$ structure was obtained by taking a quadruple cell from the original structure (corresponding to a $Li_{24}B_{72}(Li_2O)_4$ global composition starting from occupancies of 1 for all atoms) and removing 4 Li2 atoms among 20 atoms, 2 Li3 atoms among 4 atoms, and 3 oxygen atoms among 4 atoms in this supercell to obtain a $Li_{24}B_{72}(Li_2O)$ global composition. The same procedure was applied to a double cell to obtain the $Li_6B_{18}(Li_2O)_{0.5}$ structure. In addition, starting from another structure proposed by Nesper *et al*[10] for a global $Li_6B_{18}(Li_2O)_{0.70}$ composition (**Table S2**), the third model $Li_6B_{18}(Li_2O)_{0.75}$ was obtained taking a quadruple cell from the original structure (corresponding to a $Li_{52}B_{72}(Li_2O)_4$ global composition starting from occupancies of 1 for all atoms) and removing 18 Li2 atoms among 32 atoms, 18 Li3 atoms among 24 atoms, 2 Li4 atoms among 4 atoms, and one oxygen atoms among 4 atoms in this supercell to obtain a $Li_{24}B_{72}(Li_2O)_3$ global composition. The atomic positions in these supercells were then DFT-relaxed (See Methods section for details) before calculation of NMR parameters with the gauge including projector augmented wave method. The results are summarized in **Tables S3-5** and **Figures S3-5**. ^{7}Li NMR parameters for Li2 and Li3 sites (green and yellow atoms in the largest channels, **Figure 2**) are calculated between -1.6 and -0.2 ppm in $Li_6B_{18}(Li_2O)_{0.5}$ and between -1.5 and 0.2 ppm in $Li_6B_{18}(Li_2O)_{0.25}$ (details **Figure S6**), in agreement with the main signal experimentally observed around 0 ppm while half of the Li1 sites (purple atoms in the thinnest channels,

Figure 2) are calculated around -4 ppm, in accordance with the less intense experimental signal. In a similar manner, in the case of $Li_6B_{18}(Li_2O)_{0.75}$, 2/3 of Li1 sites are calculated around -4 ppm in agreement with the less intense signal, while ^{7}Li NMR parameters for Li2, Li3 and Li4 sites were calculated between -1 and 1.2 ppm, in the range of the more intense signal. Overall, comparison of the calculated and experimental ^{7}Li solid-state NMR spectra shows a satisfying agreement for x = 0.25, 0.5 and 0.75 and then does not allow a clear determination of the x value. A more precise evaluation of the composition could not be reached because of the high sensitivity of the powder to exposure to air, which is exacerbated by the nanoscale compared to the bulk material.[10]

The complex ^{11}B solid-state NMR signal (**Figure 4B**) is the superimposition of the two crystallographically inequivalent boron atoms into the $Li_6B_{18}(Li_2O)_x$ structure from the equatorial (B1) and the apical (B2) positions in the B_6 octahedra. Calculated ^{11}B NMR parameters (**Tables S3-5)** and **Figure S3-5**, details **Figure S6**) show that B1 sites appear at higher chemical shift values, typically between 1.4 and 8.1 ppm or between 1.9 and 6.3 ppm in $Li_6B_{18}(Li_2O)_{25}$ and $Li_6B_{18}(Li_2O)_{0.75}$ models respectively. B2 sites are expected between -12.6 and -1.6 ppm in $Li_6B_{18}(Li_2O)_{0.25}$ and between -13.8 and –0.5 ppm in $Li_6B_{18}(Li_2O)_{0.75}$. These parameters are not able to reproduce very accurately the experimental spectrum but since ^{11}B calculated quadruplar coupling constants seem very small while boron atoms are close in space, the spectrum shape is probably dominated by dipolar couplings, which were not taken into account by the calculation. This most likely explains the additional contribution around 20 ppm (**Figure 4B**). Note however that the presence of an impurity containing boron cannot be completely excluded.

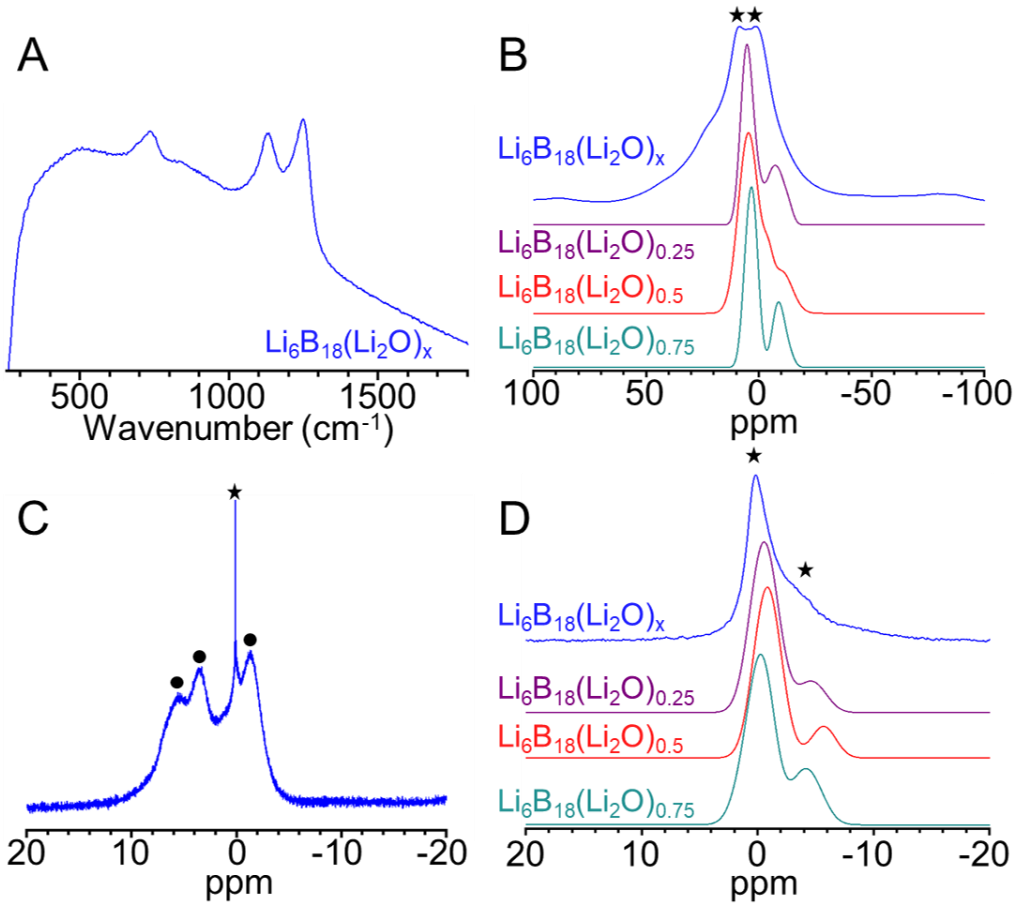

Figure 4. (A) Raman spectrum of the $Li_6B_{18}(Li_2O)_x$ powder. (B) ^{11}B, (C) ^{1}H, and (D) ^{7}Li experimental solid-state NMR spectra of $Li_6B_{18}(Li_2O)_x$ (blue). The calculated spectra of $Li_6B_{18}(Li_2O)_{0.25}$,of $Li_6B_{18}(Li_2O)_{0.5}$ and $Li_6B_{18}(Li_2O)_{0.75}$ are shown in purple and red, respectively (Details of the individual components of the fits are shown in **Figure S6**).

Scanning and transmission electron microscopies (SEM and TEM) (**Figure 5A-C**) show faceted particles with a size distribution between ca. 50 and 200 nm (**Figure 5B**). The characteristic d-spacings measured by HRTEM (**Figure 5D**) and selected area electron diffraction (SAED, **Figure 5D inset**) are consistent with the $Li_6B_{18}(Li_2O)_x$ structure. They suggest that the particles expose {100} faces. By making the hypothesis of exposed {100} faces and by taking into account the 6-fold crystal symmetry along the *c* axis, we have modelled the particles morphology with {001} and {100} sets of facets (**Figure 5E**). The corresponding projection along the [010] direction is in agreement with the TEM image in Figure 5D. The

[001] growth direction corresponds to the orientation of 6-fold channels, as in structurally related hexagonal tungsten bronzes, which typically grow along this direction.[11,12] Growth along the [001] direction to varying extent would also result in a variation of the aspect ratio of the particles, as observed for related hexagonal tungsten bronzes[11,12] and in agreement with TEM observations (Figure 5C).

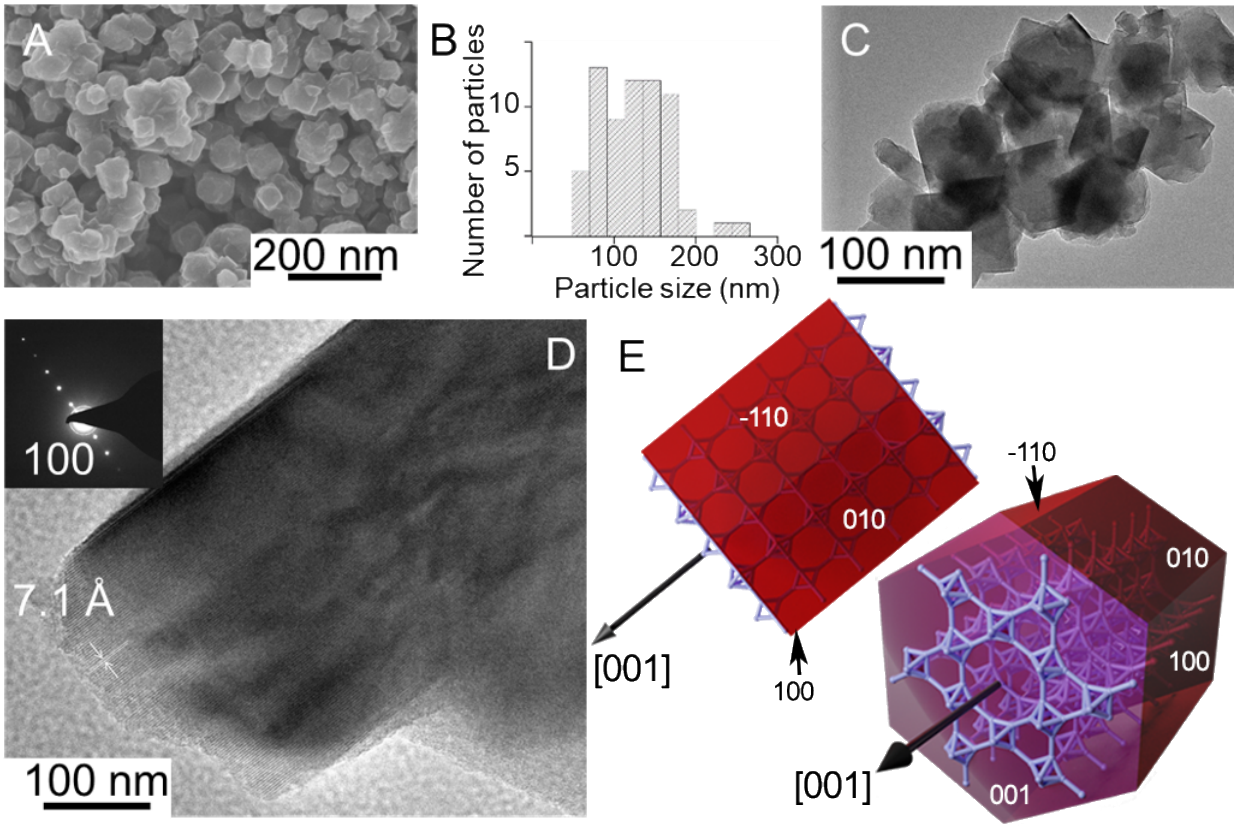

Figure 5. Electron microscopy characterization of $Li_6B_{18}(Li_2O)_x$ particles. (A) SEM image and (B) corresponding size distribution. (C) TEM image. (D) HRTEM image and corresponding SAED pattern indexed along the $Li_6B_{18}(Li_2O)_x$ structure. (E) Scheme of the morphology of the particles deduced by TEM, with indexation of facets and of the growth direction.

One remaining question is the origin of oxygen anions forming Li_2O guest species. In the original synthesis by Nesper *et al.*,[10] the porous structure could not be obtained without the

introduction of Li_2O and only Li_2B_6 was obtained instead (**Figure 1A**). No lithium oxide was used in our synthesis and the synthesis was performed under argon atmosphere. The only oxygen source here are impurities in the commercial salts LiI, KI and $NaBH_4$, such as Li_2O, LiOH, KOH and NaOH. An additional source of oxygen may be the argon gas, which is used as received without further purification.

Conclusion

$Li_6B_{18}(Li_2O)_x$ was synthesized for the first time as nanoparticles. Synthesis in inorganic molten salts enables a decrease in reaction temperature and time and a decrease in the particle size compared to solid-state reactions. The structure of this solid was confirmed by powder XRD and especially ^7Li and ^{11}B solid-state NMR for which we could propose an assignment of the complex signals. This combined solid-state NMR/DFT analysis provides references for NMR studies of lithium borides and should contribute to further structural studies of these compounds. The liquid-phase route results in $Li_6B_{18}(Li_2O)_x$ particles exhibiting an homogeneous morphology with preferential growth along the channels direction, as in structurally related tungsten bronzes. This crystal habit might have interesting consequences for electrochemical and ion exchange properties, since the Li_2O template removal from the channels has been previously demonstrated. Finally, we anticipate that the versatility of this liquid-phase synthesis pathway will lead in the future to other nanostructured alkaline borides.

Acknowledgments

NMR spectroscopic calculations were performed using HPC resources from GENCI-IDRIS (Grant 097535).

Supporting information. Figures S1 to S6, Tables S1 to S5. Crystallographic structures of $Li_{30}B_{309}$, β-B. Crystallographic data for $Li_6B_{18}(Li_2O)_{0.26}$ and $Li_6B_{18}(Li_2O)_{0.7}$. Calculated ^{11}B and ^7Li NMR parameters and spectra for the $Li_6B_{18}(Li_2O)_{0.5}$, $Li_6B_{18}(Li_2O)_{0.25}$ and $Li_6B_{18}(Li_2O)_{0.75}$ models.

References

(1) Albert, B. The Structure Chemistry of Boron-Rich Solids of the Alkali Metals. *Eur. J. Inorg. Chem.* **2000**, *2000*, 1679–1685. https://doi.org/10.1002/1099-0682(200008)2000:8<1679::AID-EJIC1679>3.3.CO;2-B.

(2) Mair, G.; Nesper, R.; von Schnering, H. G. Trilithium Tetradecaboride Li3B14: Synthesis, Structure, and Properties. *J. Solid State Chem.* **1988**, *75*, 30–40. https://doi.org/10.1016/0022-4596(88)90300-3.

(3) Mair, G.; von Schnering, H. G.; Wörle, M.; Nesper, R. Dilithium Hexaboride, Li2B6. *Zeitschrift für Anorg. und Allg. Chemie* **1999**, *625*, 1207–1211. https://doi.org/10.1002/(SICI)1521-3749(199907)625:7<1207::AID-ZAAC1207>3.0.CO;2-9.

(4) Wörle, M.; Nesper, R. Infinite, Linear, Unbranched Borynide Chains in LiBx—Isoelectronic to Polyyne and Polycumulene. *Angew. Chem. Int. Ed.* **2000**, *39*, 2349–2353. https://doi.org/10.1002/1521-3773(20000703)39:13<2349::AID-ANIE2349>3.0.CO;2-U.

(5) Wang, F. E. An Unusual Phenomenon in the Formation of Li5B4 Compound-Alloy. *Metall. Trans. A* **1979**, *10*, 343–348. https://doi.org/10.1007/BF02658343.

(6) Dallek, S.; Ernst, D. W.; Larrick, B. F. Thermal Analysis of Lithium - Boron Alloys Thermal Analysis of Lithium-Boron Alloys. *J. Electrochem. Soc.* **1979**, *126*, 866.

(7) Liu, Z.; Qu, X.; Huang, B.; Li, Z. Crystal Structure and Morphology of a New Compound, LiB. *J. Alloys Compd.* **2000**, *311*, 256–264. https://doi.org/10.1016/S0925-8388(00)01076-8.

(8) Kobayashi, M.; Higashi, I.; Matsuda, H.; Kimura, K. Rietveld Analysis of LiB13 with β-Rhombohedral Boron Structure. *J. Alloys Compd.* **1995**, *221*, 120–124. https://doi.org/10.1016/0925-8388(94)01438-8.

(9) Vojteer, N.; Stauffer, J.; Hillebrecht, H.; Hofmann, K.; Panda, M.; Albert, B. Lithium Intercalation into β-Rhombohedral Boron: LiB10 or Li30B309 ? *Zeitschrift für Anorg. und Allg. Chemie* **2009**, *635*, 653–659. https://doi.org/10.1002/zaac.200900111.

(10) Wörle, M.; Nesper, R.; Mair, G.; von Schnering, H. G. Li6B18(Li2O)x - A Boride with a Porous Framework of B6 Octahedra. *Solid State Sci.* **2007**, *9*, 459–464. https://doi.org/10.1016/j.solidstatesciences.2007.03.029.

(11) Zheng, H.; Ou, J. Z.; Strano, M. S.; Kaner, R. B.; Mitchell, A.; Kalantar-zadeh, K. Nanostructured Tungsten Oxide - Properties, Synthesis, and Applications. *Adv. Funct. Mater.* **2011**, *21*, 2175–2196. https://doi.org/10.1002/adfm.201002477.

(12) Besnardiere, J.; Ma, B.; Torres-Pardo, A.; Wallez, G.; Kabbour, H.; González-Calbet, J. M.; Von Bardeleben, H. J.; Fleury, B.; Buissette, V.; Sanchez, C.; et al. Structure and Electrochromism of Two-Dimensional Octahedral Molecular Sieve h'-WO3. *Nat. Commun.* **2019**, *10*, 327.

(13) Shen, Y.; Zerger, R.; DeGuzman, R.; Suib, S. L.; McCurdy, L.; Potter, D.; O'Young,

C. Manganese Oxide Octahedral Molecular Sieves: Preparation, Characterization, and Applications. *Science.* **1993**, *260* (5107), 511–515.

(14) La Mer, V. K.; Dinegar, H. Theory, Production and Mechanism of Formation of Monodispersed Hydrosols. *J. Am. Chem. Soc.* **1950**, *72*, 4847–4854.

(15) Kresse, G.; Furthmüller, J. Vienna Ab-Initio Simulation Package (VASP). Institut für Materialphysik: Vienna 2012.

(16) Giannozzi, P.; Baroni, S.; Bonini, N.; Calandra, M.; Car, R.; Cavazzoni, C.; Ceresoli, D.; Chiarotti, G. L.; Cococcioni, M.; Dabo, I.; et al. Journal of Physics: Condensed Matter QUANTUM ESPRESSO: A Modular and Open-Source Software Project for Quantum Simulations of Materials. *J. Phys. Cond. Matt.* **2009**, *21*, 395502.

(17) Perdew, J. P.; Burke, K.; Ernzerhof, M. Generalized Gradient Approximation Made Simple. *Phys. Rev. Lett.* **1996**, *77*, 3865–3868.

(18) Troullier, N.; Martins, J. L. Efficient Pseudopotentials for Plane-Wave Calculations. *Phys. Rev. B* **1991**, *43*, 1993–2006.

(19) Kleinman, L.; Bylander, D. Efficacious Form for Model Pseudopotentials. *Phys. Rev. Lett.* **1982**, *48*, 1425.

(20) Pickard, C.; Mauri, F. All-Electron Magnetic Response with Pseudopotentials: NMR Chemical Shifts. *Phys. Rev. B* **2001**, *63*, 245101.

(21) Pyykkö, P. Year-2008 Nuclear Quadrupole Moments. *Mol. Phys.* **2008**, *106*, 1965–1974.

(22) Massiot, D.; Fayon, F.; Capron, M.; King, I.; Le Calvé, S.; Alonso, B.; Durand, J. O.; Bujoli, B.; Gan, Z.; Hoatson, G. Modelling One- and Two-Dimensional Solid-State NMR Spectra. *Magn. Reson. Chem.* **2002**, *40*, 70–76. https://doi.org/10.1002/mrc.984.

(23) Yahia, Z. Infrared and Raman Spectra of Hexaborides: Force-Field Calculations, and Isotopic Effects. *J. Mol. Struct.* **1990**, *224*, 303–312. https://doi.org/10.1016/0022-2860(90)87025-S.

Table of content graphic

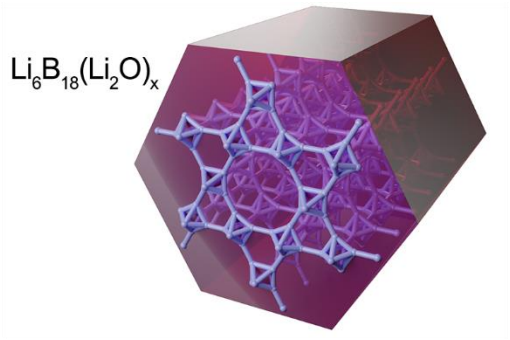

Table of content synopsis

The synthesis of nanoparticles of the lithium boride $Li_6B_{18}(Li_2O)_x$ and their in depth structural characterization are enabled by a liquid-phase pathway into inorganic molten salts.